sustainability

MDPI

Article

A Novel and Efficient Metal Oxide Fluoride Absorbent for Drinking Water Safety and Sustainable Development

Changjuan Dong [1,2], Xiaomei Wu [1,*], Zhanyi Gao [1,*], Peiling Yang [2] and Mohd Yawar Ali Khan [3]

[1] State Key Laboratory of Simulation and Regulation of Water Cycle in River Basin, China Institute of Water Resources and Hydropower Research, Beijing 100038, China; Emily_ssy@outlook.com
[2] College of Water Resources and Civil Engineering, China Agricultural University, Beijing 100083, China; yang-pl@163.com
[3] Department of Hydrogeology, King Abdulaziz University, Jeddah 21589, Saudi Arabia; yawar.gr44@gmail.com
* Correspondence: wuxm@iwhr.com (X.W.); zhanyi_gao@126.com (Z.G.); Tel.: +86-010-68786961 (X.W.); +86-010-63204693 (Z.G.)

Abstract: Inefficient and non-environmentally friendly absorbent production can lead to much resource waste and go against low carbon and sustainable development. A novel and efficient Mg-Fe-Ce (MFC) complex metal oxide absorbent of fluoride ion (F^-) removal was proposed for safe, environmentally friendly, and sustainable drinking water management. A series of optimization and preparation processes for the adsorbent and batch experiments (e.g., effects of solution pH, adsorption kinetics, adsorption isotherms, effects of coexisting anions, as well as surface properties tests) were carried out to analyze the characteristics of the adsorbent. The results indicated that optimum removal of F^- occurred in a pH range of 4–5.5, and higher adsorption performances also happened under neutral pH conditions. The kinetic data under 10 and 50 $mg \cdot g^{-1}$ were found to be suitable for the pseudo-second-order adsorption rate model, and the two-site Langmuir model was ideal for adsorption isotherm data as compared to the one-site Langmuir model. According to the two-site Langmuir model, the maximum adsorption capacity calculated at pH 7.0 ± 0.2 was 204 $mg \cdot g^{-1}$. The adsorption of F^- was not affected by the presence of sulfate (SO_4^{2-}), nitrate (NO_3^-), and chloride (Cl^-), which was suitable for practical applications in drinking water with high F^- concentration. The MFC adsorbent has an amorphous structure, and there was an exchange reaction between OH^- and F^-. The novel MFC adsorbent was proven to have higher efficiency, better economy, and environmental sustainability, and be more environmentally friendly.

Keywords: drinking water; fluoride adsorption; sustainability; tri-metal oxide absorbent

Citation: Dong, C.; Wu, X.; Gao, Z.; Yang, P.; Khan, M.Y.A. A Novel and Efficient Metal Oxide Fluoride Absorbent for Drinking Water Safety and Sustainable Development. *Sustainability* **2021**, *13*, 883. https://doi.org/10.3390/su13020883

Received: 25 November 2020
Accepted: 13 January 2021
Published: 17 January 2021

1. Introduction

Drinking water safety and sustainability, closely bound with people's lives, have always attracted the most public attention among various the human health-related issues. Fluoride pollution is one of the most common challenges in drinking water safety, and excessive fluoride intake can affect the human body and lead to severe health problems, such as fluorosis and osteoporosis [1–3]. It was reported that about 200 million people in 25 countries around the world are under the threat of the fluorosis [4]. In addition, there are nearly 45 million people suffering the negative effects of high fluoride drinking water with fluoride ion (F^-) concentrations of more than 1.0 $mg \cdot L^{-1}$ in China, mainly distributed in the north, northwest, and east of China, with 80% in the northern areas of the Yangtze River, especially in rural areas [5]. Therefore, it is an urgency to search for an effective measure to remove fluoride not only for drinking water safety and sustainability but also for the victory of a poverty alleviation plan.

Numerous efforts have been devoted to effective F^- removal technology development [6–8], such as precipitation [9], electrocagulation [10], membranes [11], ion exchange [12–14], and adsorption [15–18]. For example, Shen et al. (2003) proposed a treatment measure through the combined electrocoagulation and electroflotation process to remove fluoride ions and found that the anions had a negative effect on fluoride removal efficiency [10]. Robshaw et al. (2019) developed a novel ligand-exchange sorbent with chelating resin Purolite® S950+ loaded with lanthanum (La) ions, and it possessed a greater uptake (maximum defluoridation capacity of 187 ± 15 $mg \cdot g^{-1}$) than previously reported similar metal-loaded resins [9]. Singh et al. (2020) developed a zirconium impregnated hybrid anion exchange resin (HAIX-Zr) for fluoride removal from contaminated groundwater and evaluated fluoride removal performances. A higher defluoridation capacity (12.0 $mg \cdot g^{-1}$) and a possible fluoride removal mechanism (OH^- with F^- exchange) were found [14]. Compared with these technologies, adsorption is considered the most efficient acceptable technology due to its simple process, easy operation, and lack of pollution, and has been widely investigated in fluoride removal studies [19–21]. For example, Bansiwal et al. (2010) synthesized copper oxide coated alumina to enhance water defluoridation with a higher adsorption capacity (7.22 $mg \cdot g^{-1}$) than unmodified activated alumina (2.232 $mg \cdot g^{-1}$) [22]. Dong and Wang (2016) developed a novel lanthanum-loaded magnetic cationic hydrogel (MCH-La) for fluoride adsorption from drinking water with a maximum adsorption capacity (136.78 $mg \cdot g^{-1}$) and bigger adsorption capacity (70% from the second to fifth recycles) [23]. Thathsara et al. (2018) synthesized a novel tri-metal composite (Fe-La-Ce) for the removal of excess fluoride in aqueous media with a maximum adsorption capacity (303.03 $mg \cdot g^{-1}$ at pH 4.00) and excellent regeneration (96.13% desorption) and reusability [24]. Huang et al. (2020) proposed an Al $(OH)_3$-hydroxyapatite nanosheet (Al $(OH)_3$-nHAP) for fluoride sorption from an aqueous solution with a higher defluoridation capacity (194.2 $mg \cdot g^{-1}$ in neutral condition at 318 K) and a higher removal efficiency of a regenerated Al $(OH)_3$-nHAP nanosheet (81.32%) [25]. Kumar et al. (2020) advanced both activated alumina (AA) and grinded activated alumina (GAA) for adsorption potential by batch experiments for different contact time, pH, fluoride concentration, and adsorbent dose for fluoride adsorption [26]. From the above analysis, activated alumina is a popular treatment technology for F^- removal due to its availability and low cost, and there are some limitation on frequent regeneration with aluminum sulfate under a lower adsorption capacity at a neutral pH (5–6) [27]. Furthermore, residual alumina in treated water may cause adverse health effects due to its characteristics and 5–10% loss of adsorbency on regeneration [28].

Faced with the above difficulties, multivalent metal (Mg, Al, Fe, La, Zr) oxides and hydroxides mixed with rare earth metals have been used for obtaining higher F^- removal capacities [29–37]. This is because rare earth metals are possessed with a strong affinity for fluoride treatment [38–40].

For example, Chi et al. (2017) proposed a novel magnesium-aluminum-cerium trimetallic composite adsorbent with a higher removal efficiency over a wide range of pH (3.0–10.0) and a higher adsorption capacity for fluoride (e.g., 124.9 $mg \cdot g^{-1}$) [33]. Adak et al. (2017) developed an adsorbent with Al (III) -Fe (III) -La (III) trimetallic oxide with 99.9% fluoride removal efficiency under the condition of pH 7.0 at an adsorbent dose of 0.3 g·100 mL^{-1} during a contact time of 60 min [41]. From the previous studies, rare earth metals are commonly expensive and the optimum pH was in the acidic range. However, high fluorine drinking water is mostly alkaline. This restricts the application of the adsorbent to practical drinking water defluoridation.

Therefore, in order to search for a safe, economic, and environmentally friendly measure for practical engineering, the aim of this study was to propose a novel Mg-Fe-Ce (MFC) composite absorbent. A series of experiments of fluoride adsorption was designed to explore the characterization and mechanisms of the adsorbents, including (1) pH influence experiments for optimal pH adsorption, (2) adsorption kinetics experiments for kinetics characterization, (3) adsorption isotherm experiments for isotherm characterization, (4)

anionic influence experiments for the anionic environmental restriction of the adsorbent, and (5) X-ray diffraction (XRD) analysis and Fourier transform infrared (FTIR) spectroscopy for surface properties. The proposed MFC composite absorbent possesses the highest F^- removal capacity, lowest cost, and most environmental sustainability, and is suitable for practical applications in drinking water with a high F^- concentration.

2. Materials and Methods

2.1. Materials

All chemicals and reagents ($MgCl_2 \cdot 6H_2O$, $FeSO_4 \cdot 7H_2O$, $Ce(SO_4)_2 \cdot 4H_2O$, $Al_2(SO4)_3$, $ZnSO_4 \cdot 7H_2O$ NaF, HCl, NaOH, Na_2SO_4, NaCl, $NaNO_3$, Na_2SO_4) were of analytical grade and were mainly purchased from Chemical Engineering Company in Beijing, China; Xilong Scientific Co., Ltd.; Tianjin Guangfu Fine Chemical Research Institute; and Beijing Yili Fine Chemicals Co., Ltd. All solutions were prepared with deionized water (Total organic carbon (TOC) of less than 50 ppb, resistivity of more than 1.0 MΩ·cm, and silicide concentration of less than 100 ppb) at room temperature. The pH of the solution was measured using a pH meter (HM-14P, TOA, Kobe, Japan). F^- concentrations were analyzed with a fluoride selective electrode connected to an ion meter (IM-40S, TOA, Kobe, Japan). The dried adsorbent powder was analyzed by X-ray diffractometer (XRD, Bruker D8 Advance, Karlsruhe, Germany) and Fourier Transform Infrared Spectrometer (FTIR, Nicolet 750 model, Madison, USA).

2.2. Methods

In this study, a typical adsorbent preparation and characterization test process was proposed for F^- removal from practical drinking water engineering with high F^- concentrations. It included three steps, such as optimization of the adsorbent, preparation of the adsorbent, and experiments for adsorbent characterization. The first step was optimization of the metal components, the solution pH, the preparation method, and the calcination temperature with the objective of acquiring an adsorbent with the highest adsorption capacity. The second step was controlling the preparation condition, such as dried temperature, calcined temperature, and time, to guarantee the adsorbent preparation. The third step was carrying out the adsorption experiments and surface properties tests in order to investigate the characterization of the adsorbent. The sketch map for the process is shown in Figure 1.

2.2.1. Optimization and Preparation of the Adsorbent

To prepare the optimal adsorbent for F^- removal, a series of experiments to analyze the metal composition of the adsorbent, search for the optimization method of the adsorbent preparation, investigate the best composition ratio of the adsorbent, obtain the suitable final pH value, and determine the best calcination temperature was carried out.

In order to investigate the effect of the different metal composition of the adsorbent, three mixed solutions were prepared. The preparation processes of Mg-Fe-Ce, Zn-Al-Ce, and Zn-Fe-Ce adsorbent were the same. $MgCl_2 \cdot 6H_2O$, $FeSO_4 \cdot 7H_2O$ and $Ce(SO_4)_2 \cdot 4H_2O$ were dissolved for the mixed solution with a molar concentration ratio of Mg:Fe:Ce of 4:1:1. $ZnSO_4 \cdot 7H_2O$, $Al_2(SO4)_3$, and $Ce(SO_4)_2 \cdot 4H_2O$ were dissolved for the mixed solution with a molar concentration ratio of Zn:Al:Ce of 4:1:1. $ZnSO_4 \cdot 7H_2O$, $FeSO_4 \cdot 7H_2O$, and $Ce(SO_4)_2 \cdot 4H_2O$ were dissolved for the mixed solution with a molar concentration ratio of Zn:Fe:Ce of 4:1:1. The final pH of the three mixed solutions were all adjusted to 8.5 with 6 $mol \cdot L^{-1}$ NaOH. Then the three adsorbents (i.e., Mg-Fe-Ce, Zn-Al-Ce, and Zn-Fe-Ce) were synthesized by the co-precipitation method at a calcination temperature of 600 °C.

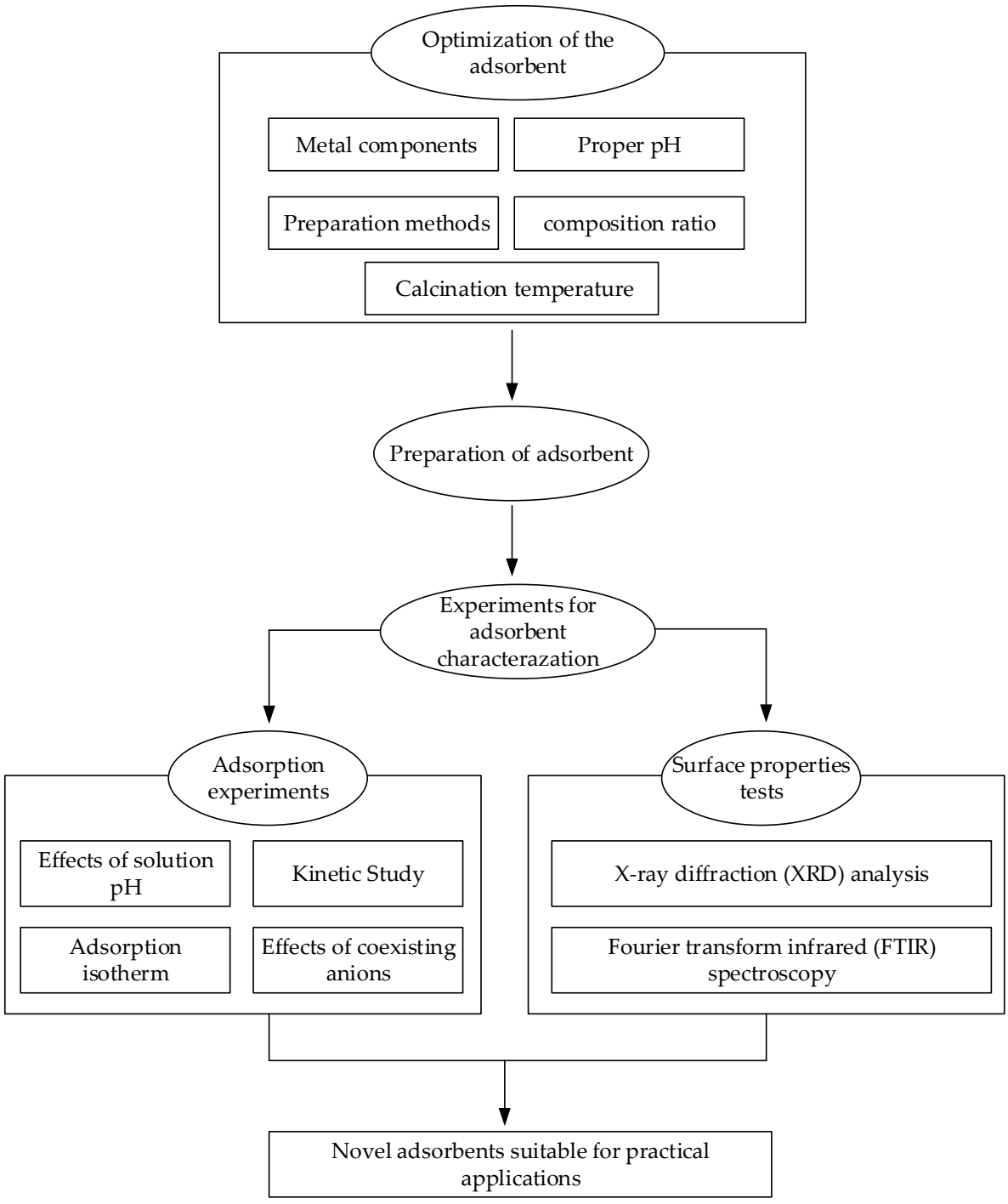

Figure 1. The sketch map of the study.

To choose the best synthetic method for the adsorbent, two synthesis methods (i.e., the co-precipitation method and hydrothermal synthesis method) were compared. The detailed co-precipitation method was (1) preparing the required experimental solution, (2) adjusting pH with 6 mol·L^{-1} NaOH to 8.5 and keeping this pH more than 30 min, (3) keeping still for more than 24 h, (4) washing the acquired precipitate and centrifuging all the mixed solution—including precipitate and washing water, (5) drying the precipitate under 65 °C for 24 h, and (6) calcining in the muffle furnace at 600 °C. The detailed hydrothermal synthesis method was (1) preparing the required experimental solution, (2) adding the solution and 6mol·L^{-1} NaOH to the autoclave and fastening the gap, (3)

heating for 6 h under 90 °C, (4) sampling after cooling and exhausting, (5) washing the acquired precipitate and centrifuging all the mixed solution—including precipitate and washing water, (6) washing and drying the precipitate under 65 °C, and (7) calcining in the muffle furnace at 600 °C.

To investigate the best composition ratio of the adsorbent, different Mg:Fe:Ce composition ratio solutions were prepared by the method of keeping two composition ratio invariant and the third composition variable (shown in Table 1). Then different composition ratio adsorbents were synthetized based on the solution with a different composition ratio at the final pH of 8.5 by co-precipitation method.

Table 1. Composition ratio of the absorbents.

Sample No.	Composition Ratio of Ce:Fe:Mg
1	0.1:0.1:0.2
2	0.1:0.1:0.4
3	0.1:0.1:0.8
4	0.05:0.1:0.4
5	0.08:0.1:0.4
6	0.10:0.1:0.4
7	0.12:0.1:0.4
8	0.10:0.05:0.4
9	0.10:0.1:0.4
10	0.10:0.15:0.4

To obtain the suitable final pH, three solutions all with a Mg:Fe:Ce molar concentration ratio of 4:1:1 were prepared. Then the final pH of the three solution was adjusted by 6 mol·L^{-1} NaOH to 8.5, 9.0, and 9.5, respectively. After that the solutions with various pHs were used to synthetize the adsorbents by the co-precipitation method.

To determine the best calcination temperature, the solution with a Mg:Fe:Ce molar concentration ratio of 4:1:1 was prepared. The final pH of the solution was adjusted by 6 mol·L^{-1} NaOH to 8.5. Then the solution was used to synthetize the adsorbent by the co-precipitation method. After that, the adsorbents were calcined in the muffle furnace at various temperatures for 3 h, such as 100 °C, 200 °C, 300 °C, 400 °C, 450 °C, 500 °C, 600 °C, 700 °C, and 800 °C.

Finally, the adsorbents obtained were put into fluoride solutions with a pH of 7.0, and then they were all put into a constant temperature oscillation incubator with a temperature of 25 °C and an oscillation velocity of 120 rpm for 24 h. The solutions after adsorption were filtered by cellulose acetate membrane filters (0.45 μm) and the F^- concentrations were measured for the adsorption capacity.

2.2.2. Fluoride Adsorption Experiments

pH Influence Experiments

Firstly, a 100 mL solution with an F^- concentration of 10 mg·L^{-1} and a 100 mL solution with an F^- concentration of 50 mg·L^{-1} were prepared. Secondly, two adsorbent samples each with a weight of 15 mg were added to the two solutions to obtained two absorbent doses of 150 mg·L^{-1}. The pH was then adjusted within the range of 3.0–10.0 by 0.1 mol·L^{-1} hydrochloric acid and 0.1 mol·L^{-1} sodium hydroxide. Finally, all the solutions were placed into a constant temperature oscillation incubator with a rotation of 120 rpm at 25 °C for 24 h.

Adsorption Kinetics Experiments

NaF was dissolved in distilled water to prepare an F^- stock solution with an F^- concentration of 1000 mg·L^{-1}. The F^- concentrations of 10 mg·L^{-1} and 50 mg·L^{-1} were prepared by diluting the solution with an F^- concentration of 1000 mg·L^{-1}. The obtained MFC adsorbent was added to the two solutions to maintain the absorbent dose

of 150 mg·L^{-1}. The pH was then adjusted to 7.0 ± 0.2, and the samples were collected at different time intervals for 24 h.

Adsorption Isotherm Experiment

NaF was dissolved in distilled water to prepare several solutions, with initial F^- concentration of 2 to 40 mg·L^{-1}. The obtained MFC adsorbent was added to each test solution to maintain the absorbent dose of 150 mg·L^{-1}. The pH was then adjusted to 7.0 ± 0.2. Finally, they were shaken at a rotation of 120 rpm and kept at 25 °C for 24 h.

Anionic Influence Experiments

Anionic solutions with initial Cl^- and $SO_4{}^{2-}$ concentrations of 10–250 mg·L^{-1}, initial $NO_3{}^-$ concentrations of 5–100 mg·L^{-1}, and initial $PO_4{}^{3-}$ concentrations of 1–50 mg·L^{-1} were prepared. NaF was dissolved in each solution to maintain the initial F^- concentration of 10 mg·L^{-1}. The MFC adsorbents were added to fix the MFC adsorbent dose of 150 mg·L^{-1}. The pH of each sample was then adjusted to 7.0 ± 0.2. They were then placed in a constant temperature oscillation incubator, shaken at 120 rpm, and kept at 25 °C for 24 h.

2.2.3. Surface Properties Tests

The surface properties of an adsorbent are the decisive factors that affect the adsorption properties. To further analyze the adsorption mechanism of the prepared adsorbent, the surface properties of the adsorbent were tested. The XRD method was used for the crystalline structure of the adsorbents through an X-ray powder diffractometer with a Cu Kα source under a scanning rate of 4°·min^{-1} in the 2θ ranging from 10° to 70° and operated at 40 kV and 100 mA. An FTIR spectrometer was applied for FTIR analysis of the adsorbent.

2.2.4. Calculation of Equilibrium Adsorption Capacity

The equilibrium adsorption capacity of the adsorbent is an important indicator that affects the performance of the adsorbent. It can be expressed as follows. [25]

$$Q_e = \frac{(C_0 - C_e)V_0}{m} \quad (1)$$

where Q_e is the equilibrium adsorption capacity of the adsorbent (mg·g^{-1}); C_0 and C_e are the initial and final F^- concentrations (mg·L^{-1}), respectively; V_0 is the volume of the solution (L); and m is the mass of the adsorbents (g).

3. Results

3.1. Optimization of the Adsorbent

The obtained results from the experiments for optimizing the metal composition, the preparation methods, the proper pH, and the calcination temperature of the adsorbent are shown in Figure 2a–d. In general, under the various initial F^- concentrations from 0–40 mg·L^{-1}, the equilibrium adsorption capacity of the three metal compositions is shown as an order of Mg-Fe-Ce > Zn-Al-Ce > Zn-Fe-Ce. Meanwhile, the adsorbents with MFC metal components exhibited significant advantages in equilibrium adsorption capacity under various initial F^- concentrations compared with the Zn-Fe-Ce adsorbent and Zn-Fe-Ce adsorbent. Therefore, Mg, Fe, and Ce were selected as the optimal metal components of the adsorbent.

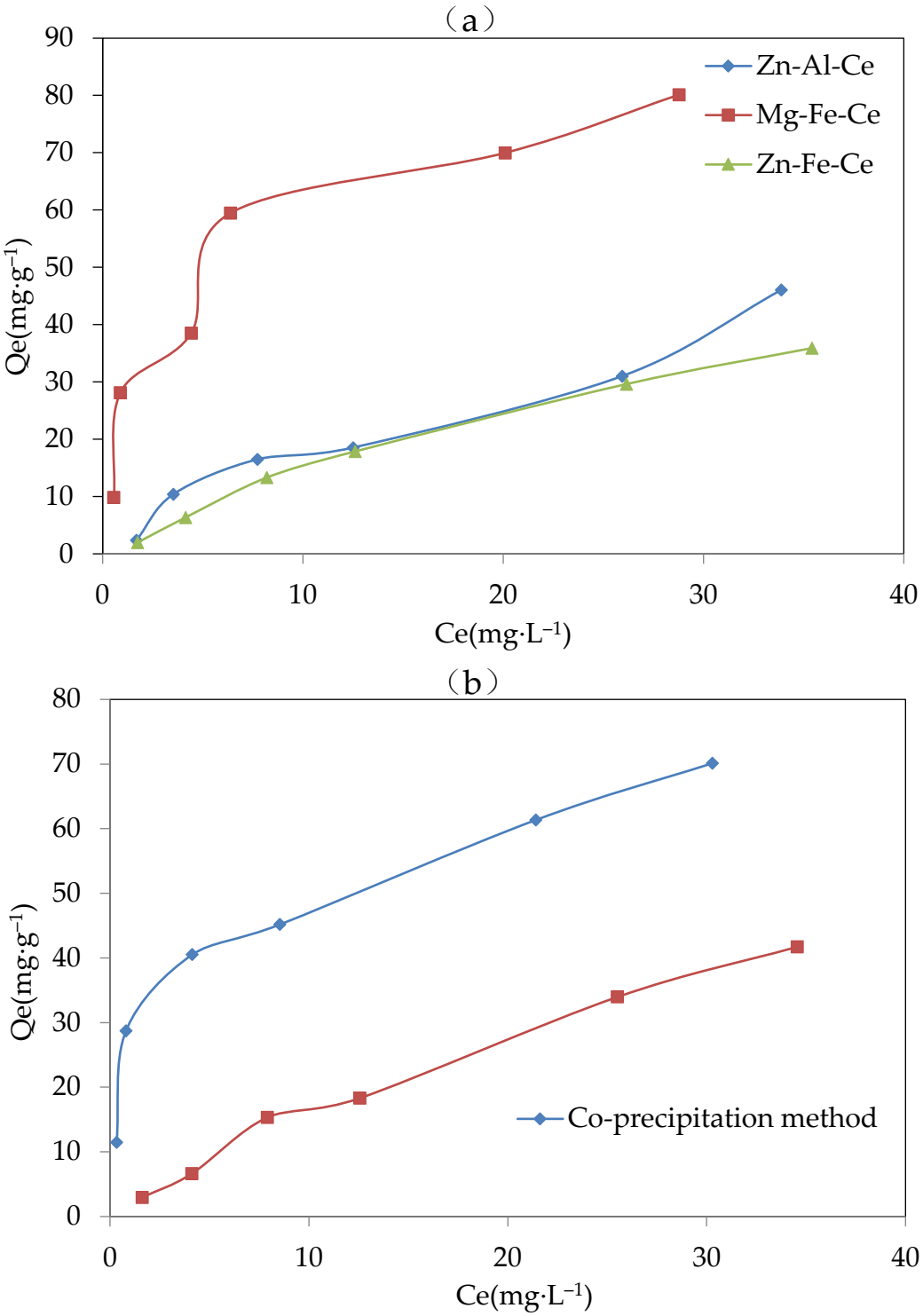

Figure 2. *Cont*.

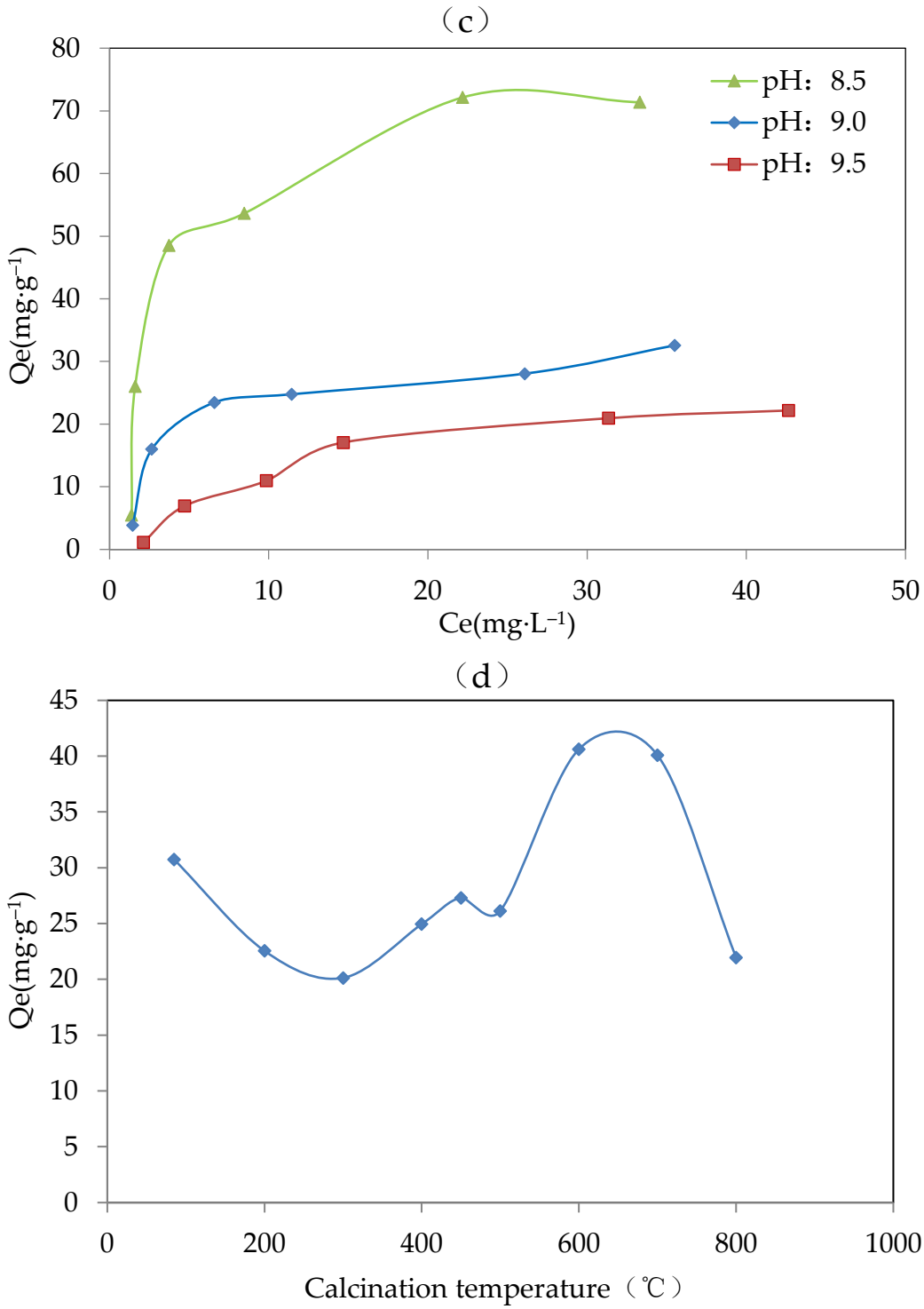

Figure 2. Results of the adsorbent optimization for (**a**) metal components (pH, 8.5; method, co-precipitation; and calcination temperature, 600 °C), (**b**) preparation methods (adsorbent, Mg-Fe-Ce; pH, 7; and temperature, 600 °C), (**c**) proper pH (adsorbent, Mg-Fe-Ce; method, co-precipitation; and calcination temperature, 600 °C), and (**d**) calcination temperature (adsorbent, Mg-Fe-Ce; pH, 7; and method, co-precipitation).

Compared with the adsorbent prepared by the hydrothermal synthesis method, the adsorbent prepared by the co-precipitation method had obvious advantages in the equilibrium adsorption capacity. The equilibrium adsorption capacity of the adsorbent made by the co-precipitation method was twice that of the adsorbent made by the hydrothermal

synthesis method. This might be because the mixed solution for the adsorbent was stirred completely in the co-precipitation method, unlike in the hydrothermal method. The adsorbent prepared by the co-precipitation method could possess more adsorption sites and a stronger adsorption capacity. Therefore, the co-precipitation method was chosen as the adsorbent preparation measure.

The equilibrium adsorption capacity under a pH value of 8.5 was significantly greater than that with a pH value of 9.0 and 9.5. This might be because there was more hydroxyl ion in the solution with the higher final pH. The environment with a higher concentration of hydroxyl ion could promote the complete precipitation process, which was unfavorable for the existence of various valence states of the same metal ion. However, the existence of various valence states of the same metal ion was helpful for fluoride adsorption. Therefore, the low adsorption activity of the adsorbent was exhibited at a pH above 8.5. Finally, the appropriate pH value for preparing the adsorbent was set to 8.5.

The calcination temperature could destroy the amorphous structure, and thereby affect the F^- removal effect. From Figure 2d, it was indicated that when the calcination temperature was 600 °C, the value of the equilibrium adsorption capacity was the highest at about 40.62 $mg \cdot g^{-1}$. The results showed that the adsorbent produced at 600 °C had better adsorption capacity. Therefore, 600 °C was chosen as the optimal calcination temperature.

In addition, the equilibrium adsorption capacity (Qe) of adsorbents with different composition ratios were compared. It was found that the adsorbent with a Mg:Fe:Ce composition ratio of 4:1:1 can possess a higher Qe value. For example, three solutions with Mg:Fe:Ce molar concentrations of 0.4:0.1:0.08, 0.2:0.1:0.10, and 0.8:0.1:0.12 were prepared and the corresponding adsorbents were synthesized by the co-precipitation method. When the adsorption experiments were carried out, the adsorbent with a Mg:Fe:Ce composition ratio of 0.4:0.1:0.10 exhibited a higher Qe value (6.79 $mg \cdot g^{-1}$) than that of the Mg:Fe:Ce composition ratios of 0.4:0.1:0.08 (3.43 $mg \cdot g^{-1}$) and 0.4:0.1:0.12 (2.80 $mg \cdot g^{-1}$). Therefore, 4:1:1 was chosen as the optimal the composition ratio of Mg:Fe:Ce.

Given that all the optimal parameters (i.e., metal composition, preparation method, composition ratio, final pH, and calcination temperature) for the preparation of the adsorbent were obtained, the MFC adsorbent was prepared. The detailed preparation processes was as follows. Firstly, 20.3 g $MgCl_2 \cdot 6H_2O$, 6.95 g $FeSO_4 \cdot 7H_2O$, and 10.10 g Ce $(SO_4)_2 \cdot 4H_2O$ were dissolved in 250 mL deionized water. Then they were stirred with a magnetic stirrer until completely dissolved to obtain an initial mixed solution for the absorbent. It took about 30 min. Then, the NaOH solution with a molar concentration of 6 $mol \cdot L^{-1}$ was used to adjust the final solution pH of 8.5 and the final pH lasted more than 30 min. After that, the solution was left for 24 h at room temperature in order to obtain the precipitate completely. The precipitate was then washed several times with distilled water and centrifuged. The residue after centrifugation was dried in an oven at a temperature of 65 °C for 24 h and then ground to MFC adsorbent power. The MFC adsorbent power was calcined at 600 °C in a muffle furnace for 3 h.

3.2. Effects of Solution pH

For F^- adsorption, pH is considered to be one of the key factors that determines the adsorption performance of the adsorbent. To investigate the influence of pH on the adsorption performance of MFC adsorbents, two initial F^- concentrations (10 $mg \cdot L^{-1}$ and 50 $mg \cdot L^{-1}$) were designed under a pH range of 3–10. As shown in Figure 3, the results indicated that under various pH values, the equilibrium adsorption capacity of the solution usually decreased as the pH value increased, and the equilibrium adsorption capacity under 50 $mg \cdot L^{-1}$ was higher than that under 10 $mg \cdot L^{-1}$. In addition, for the solution with an initial F^- concentration of 10 $mg \cdot L^{-1}$, the maximum equilibrium adsorption capacity (65 $mg \cdot g^{-1}$) could be obtained at pH 4–5.5, which was chosen as the optimal pH. For the solution with an initial F^- concentration of 50 $mg \cdot L^{-1}$, the maximum equilibrium adsorption capacity (152 $mg \cdot g^{-1}$) was obtained at a pH below 3.0. The optimal pH tended to be acidic. However, higher adsorption performances also happened under neutral

pH conditions. The results were similar to the results of Xu et al. (2001) and Zhou et al. (2004) [39,42].

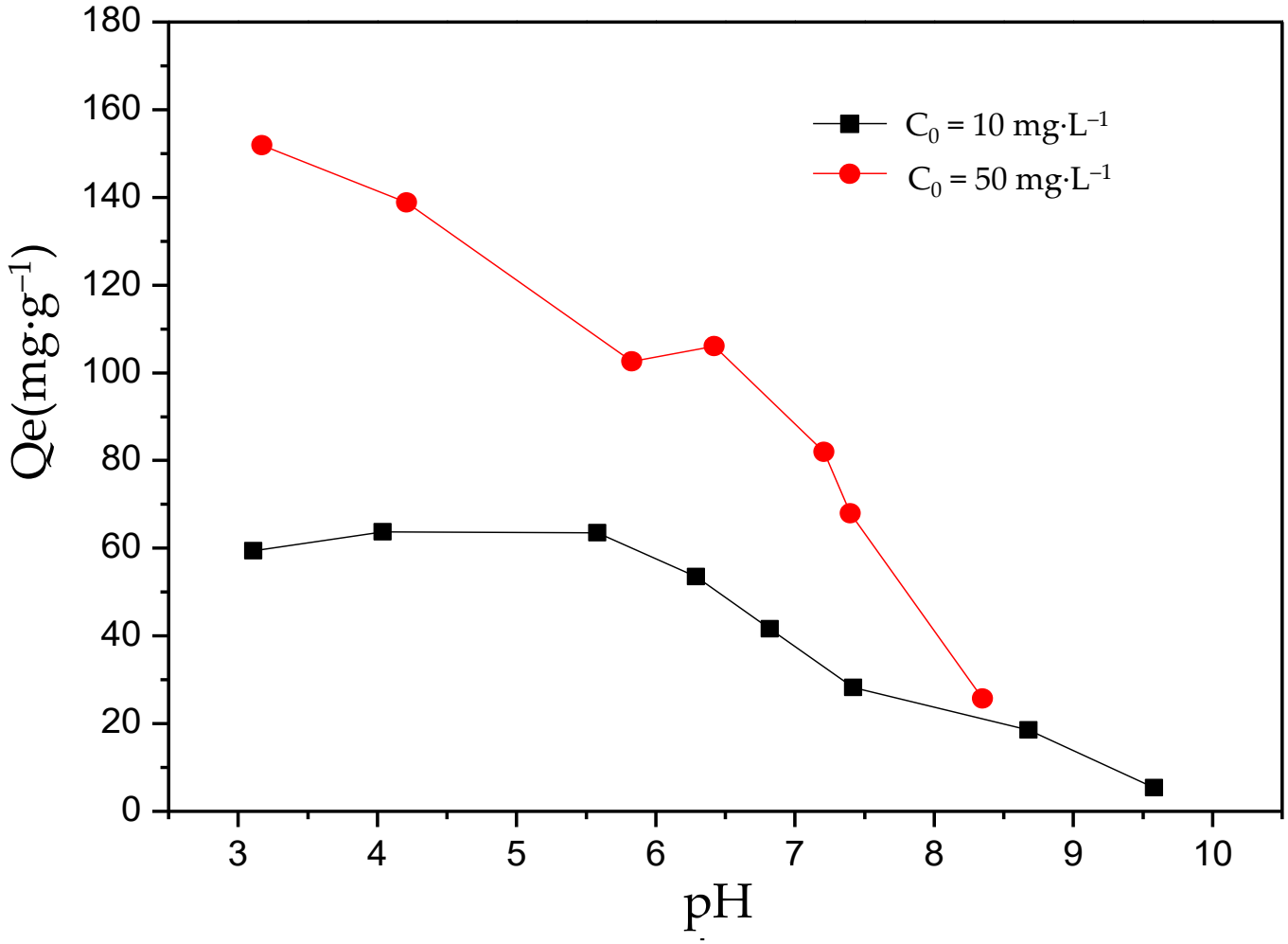

Figure 3. The effect of pH on the adsorption of fluorine by the MFC adsorbent.

From this point, as the pH value increased, the free hydroxide ions increased and could be combined with the active sites on the absorbent, occupying these sites, and hindering the combinations between F^- and the active sites, which directly resulted in a decrease in the F^- absorption amount. Meanwhile, pH value affected the charge on the surface of the adsorbent. There were two possible situations: (1) As the pH value increased, the positive charge on the surface of the absorbent became negative, or (2) the positive charge on the surface of the absorbent increased as the pH value decreased. Both of these weakened the electrostatic adsorption and cause a decrease in the adsorption capacity. In addition, the absorbent maintained a high absorption level in the neutral environment. For example, when the initial F^- concentrations were 10 $mg \cdot L^{-1}$ and 50 $mg \cdot L^{-1}$, the absorption amounts were 35 $mg \cdot g^{-1}$ and 90 $mg \cdot g^{-1}$, respectively. This indicated that the novel MFC adsorbent can be used to remove F^- from high fluoride water.

3.3. Kinetic Study

Figure 4 shows the kinetic curves of F^- adsorption under different initial F^- concentrations. The adsorption capacity under different scenarios had the same trend of variation, and the adsorption rates were fast in the first 240 min. For example, when the initial F^- concentrations were 10 $mg \cdot L^{-1}$ and 50 $mg \cdot L^{-1}$, the adsorption capacity under the first 240 min accounted for 83% and 95% of the equilibrium adsorption capacity of the solution,

respectively. The maximum F^- adsorption capacities were 40 mg·g^{-1} and 75 mg·g^{-1} for the initial F^- concentrations of 10 mg·L^{-1} and 50 mg·L^{-1}, respectively, and remained unchanged for 720 min (12 h). This may be because the F^- concentrations were at a higher level at the beginning of the F^- absorption process, and more active adsorption sites on the adsorbent worked than other processes. In the first 240 min, the adsorption driving force was large, and that drove a rapid adsorption process. In addition, part of the F^- was adsorbed by the adsorbents and the F^- concentrations decreased during the adsorption process. At the same time, the number of active adsorption sites was reduced due to the binding of F^-. The reduction in the driving force resulted in a reduction in the adsorption rate for 720 min. Due to the balance of F^- desorption and adsorption, the adsorption rate remained unchanged, and the adsorption capacity reached the highest value after 720 min.

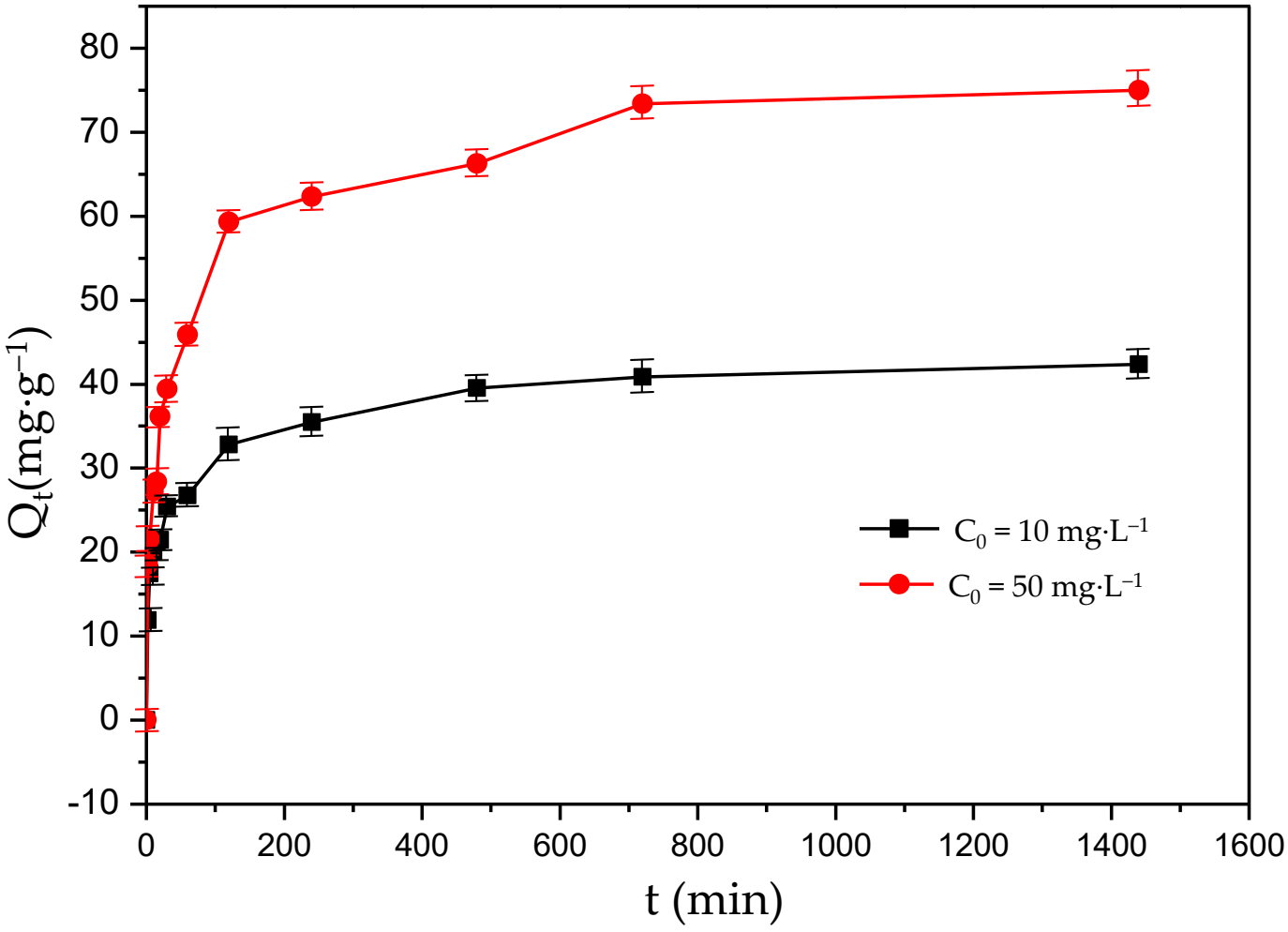

Figure 4. Kinetic curves of fluoride adsorption on the MFC adsorbent.

The pseudo-first-order rate model and pseudo-second-order rate model were applied to fit the kinetic data. They can be described as follows [17,43].

$$\log(Q_e - Q_t) = \log Q_e - k_1 t/2.303 \quad (2)$$

$$\frac{t}{Q_t} = \frac{1}{k_2 Q_e^2} + \frac{1}{Q_e} t \quad (3)$$

where Q_e (mg·g^{-1}) and Q_t (mg·g^{-1}) denote the F^- adsorption capacities at equilibrium and at any time (t), respectively; and k_1 and k_2 denote the rate constants of the pseudo-first-order and pseudo-second-order adsorption reaction, respectively. Compared with

the experimental and theoretical values of Q_e and R^2 of the kinetic curves for the pseudo-first-order rate model and pseudo-second-order model in different F^- concentrations, the pseudo-second-order model fit best. The R^2 value of the pseudo-first-order rate model and pseudo-second-order rate model were 0.9588 and 0.9989, respectively, for 10mg·L^{-1}, and 0.9482 and 0.9979, respectively, for 50 mg·L^{-1}. The best fit for the pseudo-second-order model was obtained (as shown in Figure 5), and indicated that the adsorption process might be chemisorption. The achieved rate constants (k_2) of kinetic study for 10 mg·L^{-1} and 50 mg·L^{-1} were 10.3 × 10^{-4}g·(mg·min)$^{-1}$ and 5.5 × 10^{-4} g·(mg·min)$^{-1}$, respectively. A larger rate constant means a faster adsorption process. This indicates that the adsorption process under the lower initial F^- concentration (10 mg·L^{-1}) was faster than that under the higher initial F^- concentration (50 mg·L^{-1}). The adsorption process of the MFC adsorbent may be mainly an inner-pore diffusion process.

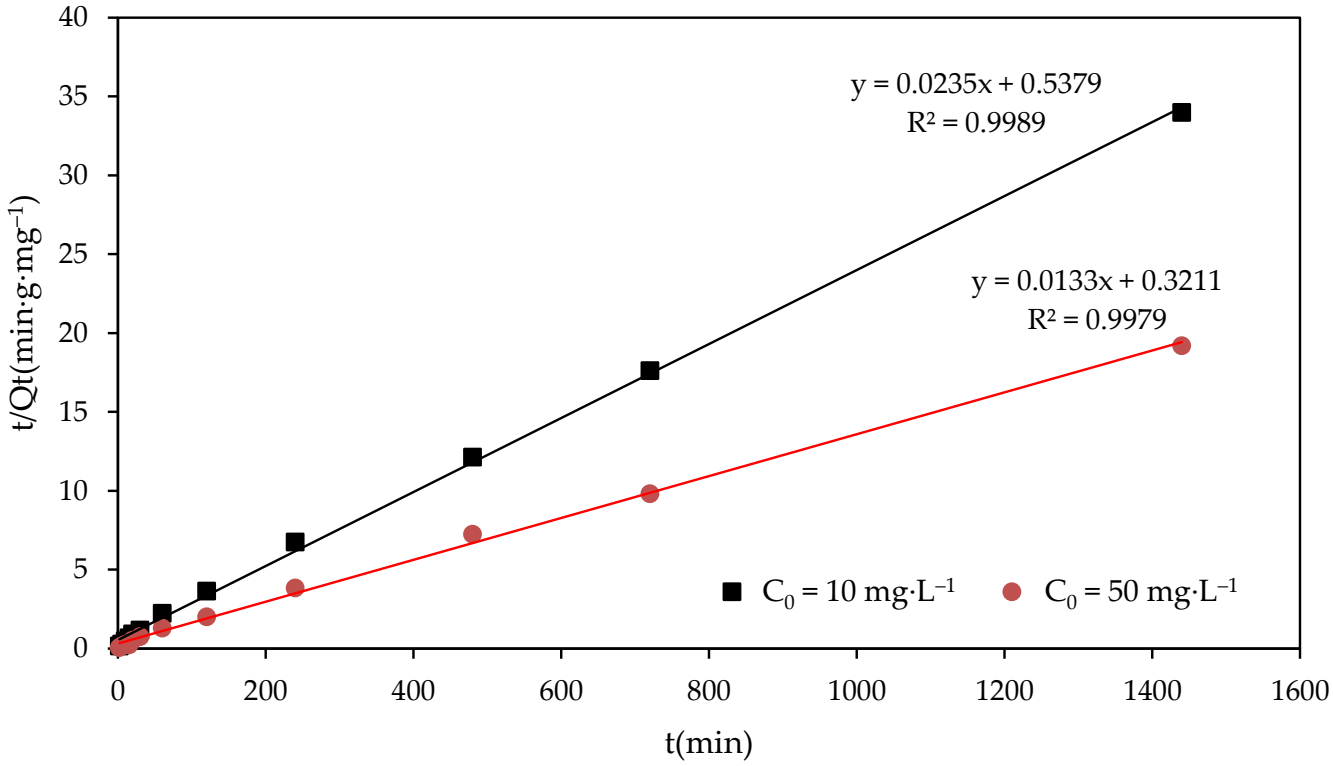

Figure 5. Kinetic curves for the pseudo-second-order model of fluoride adsorption on the MFC adsorbent.

3.4. Adsorption Isotherm

Langmuir isotherm models were applied to describe the relationship between the F^- concentration and adsorption capacity at the adsorption equilibrium. There are two Langmuir isotherm models, a one-site Langmuir model and a two-site Langmuir model. The one-site Langmuir model is based on the following assumption: Only one type of adsorption site exists on the surface of the adsorbent. The energy of the adsorption sites is the same, and there is no interaction among the adsorbed molecules in the solution. It can be described as follows:

$$Q_e = \frac{Q_{\max} b C_e}{1 + b C_e} \quad (4)$$

where Q_e (mg·g^{-1}) and $Q_{\max}$ (mg·g^{-1}) represent the equilibrium and maximum adsorption capacity, respectively; C_e (mg·L^{-1}) represents the equilibrium concentration in solution; and b (L·mg^{-1}) represents the Langmuir constant related to the adsorption–desorption affinity. The two-site Langmuir model is based on the following assumption: There are

two types of adsorption sites, one with higher affinity and other with lower affinity. It can be described as the following Equation (5):

$$Q_e = \frac{Q_1 b_1 C_e}{1 + b_1 C_e} + \frac{Q_2 b_2 C_e}{1 + b_2 C_e} \quad (5)$$

where Q_e (mg·g^{-1}), Q_1 (mg·g^{-1}), and Q_2 (mg·g^{-1}) represent the equilibrium adsorption capacity, maximum adsorption capacity at higher affinity sites, and maximum adsorption capacity at lower affinity sites, respectively; C_e (mg·L^{-1}) represents the equilibrium concentration in solution; and b_1 (L·mg^{-1}) and b_1 (L·mg^{-1}) represent the Langmuir constant related to the higher affinity and lower affinity sites, respectively.

The sorption isotherm of F^- on the Mg-Fe-Ce adsorbent with temperature (T) = 25 °C and pH = 7.0 ± 0.2 is shown in Figure 6. The corresponding parameters of the one-site and two-site Langmuir isotherm models are listed in Table 2, where Q1 and Q2 can be obtained from the calculation of the soft origin of 9.1. It was found that the experimental data were fitted not only by the one-site Langmuir isotherm model but also by the two-site Langmuir isotherm model. The correlation coefficient (R^2) of both models was greater than 0.94. However, the two-site Langmuir isotherm model gave a more satisfactory fitting result (R^2 = 0.96) than the one-site Langmuir isotherm model (R^2 = 0.94). The results showed that there may be two adsorption sites with different affinities on the surface of the MFC adsorbent. Although higher affinity sites are more likely to be occupied by F^- than lower affinity sites (b_1/b_2 = 52), a lower Q_1/Q_{max} value (30.9%) was obtained from Table 2. It was found that the adsorption capacity of lower energy sites was higher than the adsorption capacity of higher energy sites. This indicated that the active sites may be mainly sites with lower energy sites, and fewer sites with higher energy [44]. In the beginning of the adsorption, F^- was adsorbed in higher affinity sites, and the adsorption rate was fast, lasting for several minutes with little absorption (as shown in Figure 4). In addition, the experimental data showed that when the equilibrium concentration was 27 mg·L^{-1}, the adsorption capacity of F^- was 80 mg·g^{-1}. Moreover, the theoretical maximum adsorption capacity (Q_{max}) was calculated as 85 mg·g^{-1} and 204 mg·g^{-1} by one-site and two-site Langmuir models, respectively. Compared with the F^- sorption capacities of various sorbents in Table 3, the materials in this study were highly competitive compared to other products.

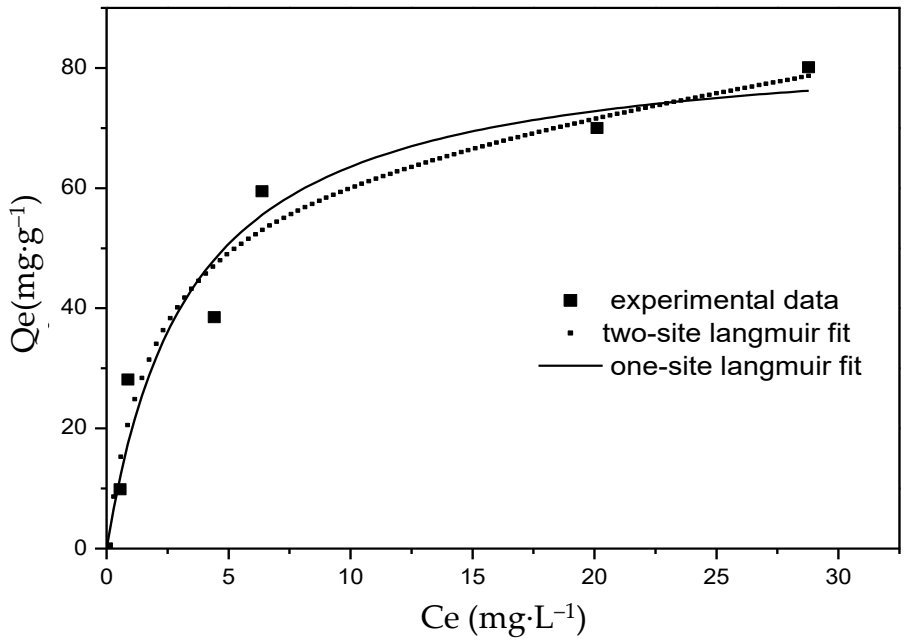

Figure 6. Fluoride adsorption isotherm at pH = 7.0 ± 0.2.

Table 2. Comparison of one-site and two-site Langmuir isotherm parameters of fluoride adsorbed from the Mg-Fe-Ce absorbent.

One-Site Langmuir			Two-Site Langmuir					
Q_{max} ($mg \cdot g^{-1}$)	b ($L \cdot mg^{-1}$)	R^2	Q_1 ($mg \cdot g^{-1}$)	Q_2 ($mg \cdot g^{-1}$)	$Q_{max} = Q_1 + Q_2$ ($mg \cdot g^{-1}$)	b_1 ($L \cdot mg^{-1}$)	b_2 ($L \cdot mg^{-1}$)	R^2
85	0.29	0.94	63	141	204	0.52	0.01	0.96

Table 3. Comparison of fluoride adsorption capacity of the MFC adsorbent with other adsorbents.

Adsorbents	pH	Q_e ($mg \cdot g^{-1}$)	References
Fe-Al-Ce composite	7.0	178	[29]
La^{3+}-exchanged zeolite F-9	7.2	54.28	[44]
Al^{3+}-exchanged zeolite F-9	5.2–5.3	39.52	[44]
Mg-Fe-Ce composite	7.0	204	Present study

3.5. Effects of Coexisting Anions

The presence of anions may be competitive for the absorption of F^-. Sulfate (SO_4^{2-}), nitrate (NO_3^-), chloride (Cl^-), and phosphate (PO_4^{3-}) are the common anions in groundwater composition. The effects of coexisting anions such as SO_4^{2-}, NO_3^-, Cl^-, and PO_4^{3-} were thereby examined. The results are given in Figure 7. It shows that even at a concentration of 100 $mg \cdot L^{-1}$, nitrate ions do not significantly interfere with the removal of F^-. SO_4^{2-} and Cl^- exhibited a similar trend. The equilibrium adsorption capacity showed a small variety when the concentrations of SO_4^{2-} and Cl^- were at a range of 5–250 $mg \cdot L^{-1}$. On the contrary, a significant variety in the equilibrium adsorption capacity of F^- was exhibited when the concentrations of PO_4^{3-} were in the range of 0–100. SO_4^{2-}, NO_3^-, and Cl^- usually had a weak influence on F^- adsorption and the influence of coexisting anion effects on F^- was arranged in the descending order of $PO_4^{3-} > SO_4^{2-} > Cl^- > NO_3^-$. The results were similar to Liu's study [45]. Additionally, PO_4^{3-} showed strong competitive adsorption with F^-. When the PO_4^{3-} concentration increased from 1 $mg \cdot L^{-1}$ to 10 $mg \cdot L^{-1}$, the equilibrium adsorption capacity decreased by about 50%, which indicated that PO_4^{3-} had a strong inhibitory effect on the adsorption of F^-. These results were also obtained in previous studies [46,47]. Therefore, more attention should be paid to the PO_4^{3-} concentration in the practical engineering application of the novel Mg-Fe-Ce adsorbent and measures should be taken for PO_4^{3-} removal. Fortunately, PO_4^{3-} concentrations in groundwater are normally low, and the effect on the F^- sorption is limited [45]. Taking all the above factors into consideration, the adsorbent prepared in this study was engineering-favorable.

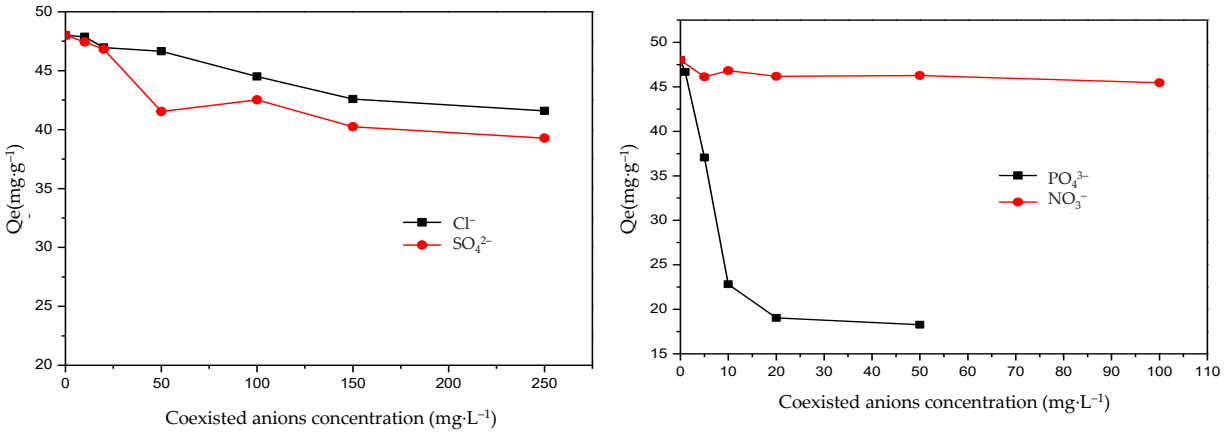

Figure 7. Effects on fluoride adsorption of coexisting anions (Qe: the equilibrium adsorption capacity of fluoride).

3.6. Surface Properties and Adsorption Mechanism Analysis

3.6.1. XRD Analysis

Figure 8 shows the XRD patterns of the MFC adsorbent for its crystal structure. It was found that there existed no crystal diffraction peaks of MFC adsorbents, and the MFC adsorbents had an amorphous structure. According to crystal chemistry, when the structure of the adsorbents was in the transition from amorphous to crystal form, more surface free energy and a thermodynamically unstable state is acquired. Oxides with surface hydroxyl groups had higher activity. Moreover, the sorption capacity was related to the amorphous structure of the adsorbents, and the destruction of the amorphous structure of the adsorbents resulted in a decrease in the adsorption capacity for F^-. Moreover, there was a large and wide peak packet from 20° to 40° at two theta angles. This can be attributed to the short-range order characterization of amorphous metal oxide.

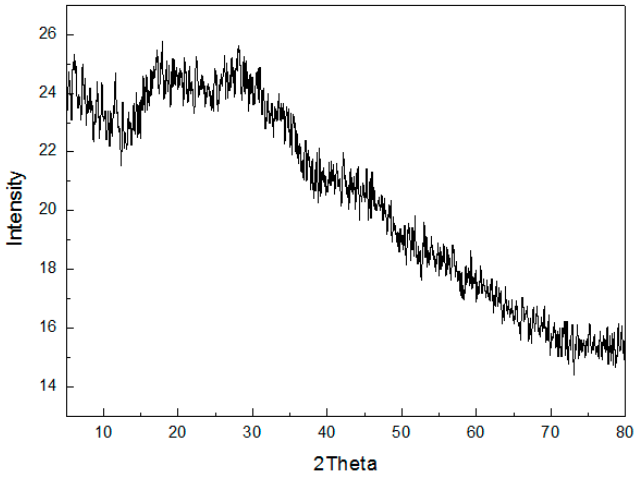

Figure 8. XRD patterns of the MFC adsorbents.

3.6.2. FTIR Spectroscopy

Figure 9 shows the FTIR spectra of MFC adsorbent samples before and after fluoride adsorption. The sample before fluoride adsorption was prepared from a solution with a final pH of 8.5 and synthesized by the co-precipitation method. The sample after fluoride adsorption was obtained after adsorption in the solution with a fluoride concentration of 400 $mg{\cdot}L^{-1}$ and the pH was 7.0. The MFC adsorbent was a composite metal oxide adsorbent with hydroxyl groups on the surface. The stretching vibration of hydroxyl groups on the metal surface usually occurred below 1200 cm^{-1}, and there was no bending vibration mode near 1600 cm^{-1}. It was found that some peaks appeared between 1200 and 0 cm^{-1} in Figure 9. They were characterized as a stretching vibration of hydroxyl groups on the metal surface. There existed a broad band at 3400 cm^{-1} in the spectrum of the Mg-Fe-Ce adsorbent. This can be attributed to the stretching vibration of adsorbed water. It indicated that the stretching vibration peak intensity of the hydroxyl groups on the adsorbent surface were significantly reduced at 1125 cm^{-1}, and an exchange reaction might have occurred between OH-and F^-. This can be explained by the similar dimensions exhibited by OH^- and F^-. In addition, there were new peaks (marked with the orange line) in the spectrum of the MFC adsorbent after fluoride adsorption. This might be explained by the formed Mg-F, Fe-F, and Ce-F bonds. Given that the surface hydroxyl groups played a vital role in F^- removal, the possible adsorption mechanism can be described as follows.

$$\equiv MOH(s) + H^+ = \equiv MOH_2^+ \quad (6)$$

$$\equiv MOH_2^+(s) + F^-(aq) = \equiv MOF(s) + H_2O \quad (7)$$

$$\equiv MOH(s) + F^-(aq) = \equiv MF(s) + OH^- \quad (8)$$

where ≡ *M* is the MFC tri-metal hydroxide.

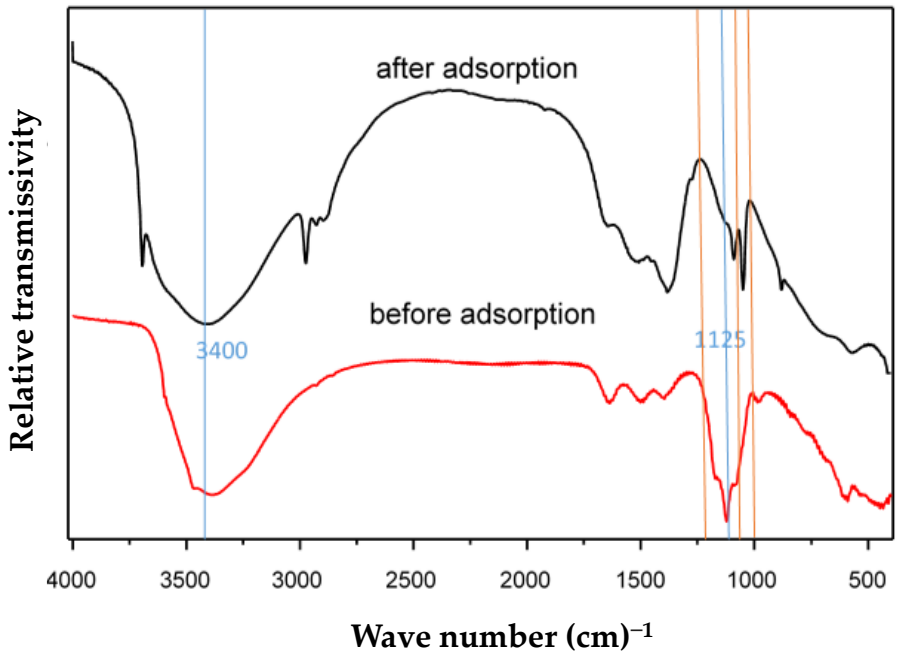

Figure 9. FTIR spectra of the MFC adsorbent.

3.7. Adsorption Mechanisms

The adsorption mechanism of fluoride adsorption could be obtained based on the adsorption experiments, XRD and FIIR analysis, and previous studies [25,44]. Generally, two mechanisms (i.e., electrostatic interaction and ion-exchange) can explain the fluoride adsorption of the MFC adsorbent. When the solution was in acid condition, the electrostatic interaction mainly dominated the sorption. That was because when the solution was in a lower pH, there was more H^+ in the solution, which led to the protonated surface of the MFC. Meanwhile, the OH^- turned into OH_2^+, which was helpful for the adsorption of F^-. However, when the solution was in an alkaline condition, the ion-exchange interaction mainly dominated the sorption. That was because when the solution was in a higher pH, there was more OH^- in the solution, which possessed similar dimensions as F^-. OH^- can play an important role in not only ion-exchange interaction with F^- but also competing with F^- for active sites, which leads to a decrease of defluoridation capacity.

4. Conclusions

In this study, in order to search for an effective, safe, and environmentally friendly measure for practical engineering, a novel MFC tri-metal oxide adsorbent was developed for F^- adsorption. Through the optimization of the adsorbent, preparation of the adsorbent, and experiments for the adsorbent characterization, the characterization and F^- adsorption mechanism of the adsorbent were tested and analyzed. The optimum pH range for F^- removal was 4–5.5, and the adsorbent was also effective at pH 7.0 with a maximum adsorption capacity of 204 mg·g^{-1}, which was highly competitive compared to other reported adsorbents. The adsorption isotherm fit better with the two-site Langmuir model than the one-site model. The presences of SO_4^{2-}, NO_3^-, and Cl^- had almost no effects on F^- adsorption of the adsorbent. It was suitable for practical applications in groundwater with high F^- adsorption with F^-.

The adsorption of F^- mainly occurs through ion exchange. MFC adsorbents have amorphous structures, and an exchange reaction between OH^- and F^- exists for enhancing the treatment capacity. The MFC tri-metal oxide adsorbent shows attractive application prospects in F^- removal and can contribute to sustainable drinking water development.

Author Contributions: Conceptualization, C.D. and X.W.; methodology, C.D. and X.W.; validation, C.D. and Z.G.; formal analysis, C.D.; investigation, C.D.; resources, X.W.; data curation, C.D.; writing—original draft preparation, C.D.; writing—review and editing, C.D. and M.Y.A.K.; supervision, Z.G. and P.Y. All authors have read and agreed to the published version of the manuscript.

Funding: This research was funded by the National Key Research and Development Programme of China (No.2018YFC0408102).

Institutional Review Board Statement: Not applicable.

Informed Consent Statement: Not applicable.

Data Availability Statement: Data that support the findings of this study are available from the corresponding author upon reasonable request.

Acknowledgments: Thanks to the support of the State Key Laboratory of Simulation and Regulation of Water Cycle in River Basin for proving convenient experimental conditions. The authors wish to thank the referees for providing helpful suggestions to improve this manuscript.

Conflicts of Interest: The authors declare no conflict of interest.

References

1. Jimenez-Farfan, M.D.; Hernandez-Guerrero, J.C.; Juarez-Lopez, L.A.; Jacinto-Aleman, L.F.; de la Fuente-Hernandez, J. Fluoride consumption and its impact on oral health. *Int. J. Environ. Res. Public Health* **2011**, *8*, 148–160. [CrossRef] [PubMed]
2. Ologundudu, T.O.; Odiyo, J.O.; Ekosse, G.I.E. Fluoride Sorption Efficiency of Vermiculite Functionalised with Cationic Surfactant: Isotherm and Kinetics. *Appl. Sci.* **2016**, *6*, 277. [CrossRef]
3. Jia, H.; Qian, H.; Qu, W.G.; Zheng, L.; Feng, W.W.; Ren, W.H. Fluoride occurrence and human health risk in drinking water wells from southern edge of Chinese Loess Plateau. *Int. J. Environ. Res. Public Health* **2019**, *16*, 1683. [CrossRef] [PubMed]
4. Cherukumilli, K.; Delaire, C.; Amrose, S.; Gadgil, A.J. Factors governing the performance of bauxite for fluoride remediation of groundwater. *Environ. Sci. Technol.* **2017**, *51*, 2321–2328. [CrossRef]
5. Wen, D.; Zhang, F.; Zhang, E.; Wang, C.; Han, S.; Zheng, Y. Arsenic, fluoride and iodine in groundwater of China. *J. Geochem. Explor.* **2013**, *135*, 1–21. [CrossRef]
6. Rudelis, V.; Dambrauskas, T.; Grineviciene, A.; Baltakys, K. The Prospective Approach for the Reduction of Fluoride Ions Mobility in Industrial Waste by Creating Products of Commercial Value. *Sustainability* **2019**, *11*, 634. [CrossRef]
7. Fawell, J.; Bailey, K.; Chilton, J.; Dahi, E.; Fewtrell, L.; Magara, Y.; World Health Organization. *Fluoride in Drinking Water*; World Health Organization (WHO): London, UK, 2006.
8. Marwa, J.; Lufingo, M.; Noubactep, C.; Machunda, R. Defeating Fluorosis in the East African Rift Valley: Transforming the Kilimanjaro into a Rainwater Harvesting Park. *Sustainability* **2018**, *10*, 4194. [CrossRef]
9. Robshaw, T.; Tukra, S.; Hammond, D.B.; Leggett, G.J.; Ogden, M.D. Highly efficient fluoride extraction from simulant leachate of spent potlining via La-loaded chelating resin. An equilibrium study. *J. Hazard. Mater.* **2019**, *361*, 200–209. [CrossRef]
10. Shen, F.; Chen, X.; Gao, P.; Chen, G. Electrochemical removal of fluoride ions from industrial wastewater. *Chem. Eng. Sci.* **2003**, *58*, 987–993. [CrossRef]
11. Chang, H.Y.H.; Kuo, Y.L.; Liu, J.C. Fluoride at waste oyster shell surfaces-Role of magnesium. *Sci. Total Environ.* **2019**, *652*, 1331–1338. [CrossRef]
12. Cai, J.G.; Zhang, Y.L.; Pan, B.C.; Zhang, W.M.; Lv, L.; Zhang, Q.X. Efficient defluoridation of water using reusable nanocrystalline layered double hydroxides impregnated polystyrene anion exchanger. *Water Res.* **2016**, *102*, 109–116. [CrossRef] [PubMed]
13. Changmai, M.; Pasawan, M.; Purkait, M.K. A hybrid method for the removal of fluoride from drinking water, parametric study and cost estimation. *Sep. Purif. Technol.* **2018**, *206*, 140–148. [CrossRef]
14. Singh, S.; German, M.; Chaudhari, S.; Sengupta, A.K. Fluoride removal from groundwater using zirconium impregnated anion exchange resin. *J. Environ. Manag.* **2020**, *263*, 110415. [CrossRef] [PubMed]
15. Camacho, L.; Torres, A.; Saha, D.; Deng, S.G. Adsorption equilibrium and kinetics of fluoride on sol–gel-derived activated alumina adsorbents. *J. Colloid Interface Sci.* **2010**, *349*, 307–313. [CrossRef] [PubMed]
16. Wu, X.M.; Zhang, Y.; Dou, X.M.; Zhao, B.; Yang, M. Fluoride adsorption on an Fe–Al–Ce trimetal hydrous oxide, Characterization of adsorption sites and adsorbed fluorine complex species. *Chem. Eng. J.* **2013**, *223*, 364–370. [CrossRef]
17. Sun, C.Z.; Qiu, J.W.; Zhang, Z.B.; Marhaba, T.F.; Zhang, Y.H. Removal of arsenite from water by Ce-Al-Fe trimetal oxide adsorbent, kinetics, isotherms, and thermodynamics. *J. Chem.* **2016**, 1–8. [CrossRef]
18. Cai, Q.Q.; Turner, B.D.; Sheng, D.C.; Sloan, S. Application of kinetic models to the design of a calcite permeable reactive barrier (PRB) for fluoride remediation. *Water Res.* **2018**, *130*, 300–311. [CrossRef]
19. Yang, Y.; Paul Chen, J. Key factors for optimum performance in phosphate removal from contaminated water by a Fe–Mg–La tri-metal composite sorbent. *J. Colloid Interface Sci.* **2015**, *445*, 303–311. [CrossRef]
20. Farrah, H.; Slavek, J.; Pickering, W.F. Fluoride interactions with hydrous aluminum oxides and alumina. *Aust. J. Soil Res.* **1987**, *25*, 55–69. [CrossRef]

21. Turner, B.D.; Binning, P.; Stipp, S.L.S. Fluoride removal by calcite: Evidence for fluorite precipitation and surface adsorption. *Environ. Sci. Technol.* **2005**, *39*, 9561–9568. [CrossRef]
22. Bansiwal, A.; Pillewan, P.; Biniwale, R.B.; Rayalu, S.S. Copper oxide incorporated mesoporous alumina for defluoridation of drinking water. *Microporous Mesoporous Mater.* **2010**, *129*, 54–61. [CrossRef]
23. Dong, S.; Wang, Y. Characterization and adsorption properties of a lanthanum-loaded magnetic cationic hydrogel composite for fluoride removal. *Water Res.* **2016**, *88*, 852–860. [CrossRef] [PubMed]
24. Thathsara, S.K.T.; Cooray, P.L.A.T.; Mudiyanselage, T.K.; Kottegoda, N.; Ratnaweera, D.R. A novel Fe-La-Ce tri-metallic composite for the removal of fluoride ions from aqueous media. *J. Environ. Manag.* **2018**, *207*, 387–395. [CrossRef] [PubMed]
25. Huang, S.M.; Hu, M.L.; Li, D.; Wang, L.P.; Zhang, C.; Li, K.; He, Q.Q. Fluoride sorption from aqueous solution using Al(OH)(3)-modified hydroxyapatite nanosheet. *Fuel* **2020**, *279*, 118486. [CrossRef]
26. Kumar, R.; Sharma, P.; Aman, A.K.; Singh, R.K. Equilibrium sorption of fluoride on the activated alumina in aqueous solution. *Desalin. Water Treat.* **2020**, *197*, 224–236. [CrossRef]
27. Ghorai, S.; Pant, K.K. Investigations on the column performance of fluoride adsorption by activated alumina in a fixed-bed. *Chem. Eng. J.* **2004**, *98*, 65–173. [CrossRef]
28. George, S.; Pandit, P.; Gupta, A.B. Residual aluminium in water defluoridated using activated alumina adsorption—Modeling and simulation studies. *Water Res.* **2010**, *44*, 3055–3064. [CrossRef]
29. Wu, X.M.; Zhang, Y.; Dou, X.M.; Yang, M. Fluoride removal performance of a novel Fe–Al–Ce trimetal oxide adsorbent. *Chemosphere* **2007**, *69*, 1758–1764. [CrossRef]
30. Tor, A.; Danaoglu, N.; Arslan, G.; Cengeloglu, Y. Removal of fluoride from water by using granular red mud, batch and column studies. *J. Hazard. Mater.* **2009**, *164*, 271–278. [CrossRef]
31. Wu, L.Y.; Zhang, G.K.; Tang, D.D. A novel high efficient Mg–Ce–La adsorbent for fluoride removal, kinetics, thermodynamics and reusability. *Desalin. Water Treat.* **2016**, *57*, 23844–23855. [CrossRef]
32. Zhou, J.; Zhu, W.K.; Yu, J.; Zhang, H.P.; Zhang, Y.D.; Lin, X.Y.; Luo, X.G. Highly selective and efficient removal of fluoride from ground water by layered Al-Zr-La Tri-metal hydroxide. *Appl. Surf. Sci.* **2018**, 920–927. [CrossRef]
33. Chi, Y.L.; Chen, Y.T.; Hu, C.L.; Wang, Y.S.; Liu, C. Preparation of Mg-Al-Ce triple-metal composites for fluoride removal from aqueous solutions. *J. Mol. Liq.* **2017**, *242*, 416–422. [CrossRef]
34. Li, L.; Zhu, Q.; Man, K.X.; Xing, Z.P. Fluoride removal from liquid phase by Fe-Al-La trimetal hydroxides adsorbent prepared by iron and aluminum leaching from red mud. *J. Mol. Liq.* **2017**, *237*, 164–172. [CrossRef]
35. Kabir, H.; Gupta, A.K.; Debnath, D. Synthesis, optimization and characterization of mesoporous Mg-Al-Fe tri-metal nanocomposite targeting defluoridation, Synergistic interaction of molar ratio and thermal activation. *J. Mol. Liq.* **2018**, *268*, 376–385. [CrossRef]
36. Ghosh, A.; Chakrabarti, S.; Biswas, K.; Ghosh, U.C. Column performances on fluoride removal by agglomerated Ce(IV)–Zr(IV) mixed oxide nanoparticles packed fixed-beds. *J. Environ. Chem. Eng.* **2015**, *3*, 653–661. [CrossRef]
37. Ramos-Vargas, S.; Alfaro-Cuevas-Villanueva, R.; Huirache-Acuna, R.; Cortes-Martinez, R. Removal of fluoride and arsenate from aqueous solutions by aluminum-modified guava seeds. *Appl. Sci.* **2018**, *8*, 1807. [CrossRef]
38. Raichur, A.M.; Basu, M.J. Adsorption of fluoride onto mixed rare earth oxides. *Sep. Purif. Technol.* **2001**, *24*, 121–127. [CrossRef]
39. Zhou, Y.M.; Yu, C.X.; Shan, Y. Adsorption of fluoride from aqueous solution on La^{3+}-impregnated cross-linked gelatin. *Sep. Purif. Technol.* **2004**, *36*, 89–94. [CrossRef]
40. Chen, L.; Wang, T.J.; Wu, H.X.; Jin, Y.; Zhang, Y.; Dou, X.M. Optimization of a Fe-Al-Ce nano-adsorbent granulation process that used spray coating in a fluidized bed for fluoride removal from drinking water. *Powder Technol.* **2011**, *206*, 291–296. [CrossRef]
41. Adak, M.K.; Sen, A.; Mukherjee, A.; Sen, S.; Dhak, D. Removal of fluoride from drinking water using highly efficient nano-adsorbent, Al(III)-Fe(III)-La(III) trimetallic oxide prepared by chemical route. *J. Alloy. Compd.* **2017**, *719*, 460–469. [CrossRef]
42. Xu, Y.M.; Ning, A.R.; Zhao, J. Preparation and defluoridation performance of activated cerium(IV) oxide/SiMCM-41 adsorbent in water. *J. Colloid Interface Sci.* **2001**, *235*, 66–69. [CrossRef] [PubMed]
43. Ho, Y.S.; McKay, G. Pseudo-second order model for sorption processes. *Process. Biochem.* **1999**, *34*, 451–465. [CrossRef]
44. Onyango, M.S.; Kojima, Y.; Aoyi, O.; Bemardo, E.C.; Matsuda, H. Adsorption equilibrium modeling and solution chemistry dependence of fluoride removal from water by trivalent-cation-exchanged zeolite fluoride ion. *J. Colloid Interface Sci.* **2004**, *279*, 341–350. [CrossRef] [PubMed]
45. Liu, H.; Deng, S.B.; Li, Z.J.; Yu, G.; Huang, J. Preparation of Al–Ce hybrid adsorbent and its application for defluoridation of drinking water. *J. Hazard. Mater.* **2010**, *179*, 424–430. [CrossRef] [PubMed]
46. Kumar, E.; Bhatnagar, A.; Ji, M.; Jung, W.; Lee, S.H.; Kim, S.J.; Lee, G.; Song, H.; Choi, J.Y.; Yang, J.S.; et al. Defluoridation from aqueous solutions by granular ferric hydroxide (GFH). *Water Res.* **2009**, *43*, 490–498. [CrossRef]
47. Viswanathan, N.; Sundaram, C.S.; Meenakshi, S. Sorption behaviour of fluoride on carboxylated cross-linked chitosan beads. *Colloid Surf. B* **2009**, *68*, 48–54. [CrossRef]